Pergamon

PII: S0360-5442(98)00026-7

Energy Vol. 23, No. 10, pp. 803–814, 1998
© 1998 Elsevier Science Ltd. All rights reserved
Printed in Great Britain
0360-5442/98 $19.00 + 0.00

A SOLAR CHEMICAL REACTOR FOR CO-PRODUCTION OF ZINC AND SYNTHESIS GAS

A. STEINFELD,† M. BRACK, A. MEIER, A. WEIDENKAFF and D. WUILLEMIN

High-Temperature Solar Technology, Paul Scherrer Institute, CH-5232, Villigen PSI, Switzerland

(Received 4 December 1997)

Abstract—A novel solar chemical reactor has been designed to perform the combined ZnO-reduction and CH_4-reforming processes. It consists of a gas-particle vortex flow confined to a solar cavity-receiver that is exposed to concentrated solar irradiation. A 5-kW reactor was fabricated and tested in a high-flux solar furnace. The design methodology and experimental program are described. Tests were conducted from 1000 to 1600 K and yielded up to 90% chemical conversion of zinc in a single pass. © 1998 Elsevier Science Ltd. All rights reserved

1. INTRODUCTION

Zn is a widely used commodity in the galvanising, pharmaceutical, and food industries. It is also an attractive solid fuel. Its specific heat is 5320 kJ/kg. It may be used to generate electricity in a Zn/air battery or fuel cell. It may also be reacted with water to produce hydrogen that can be further used for heat and/or electricity generation. Industrially, Zn is extracted from ores in carbothermic and electrolytic processes. The production of Zn is characterised by high energy consumption (35–50 GJ/mt Zn) and high concomitant environmental pollution (3–12 mt CO_2/mt Zn). World production amounts to about 7 million mt/yr and annual discharges to the atmosphere approximate 66 million mt of CO_2.‡ Carbon in the form of coke is the preferred reducing agent and also the primary source of process heat. When used exclusively as the reducing agent, the stoichiometric mass ratio of carbon consumed to Zn produced should be 0.09 [4]. Actually, commercial smelting furnaces use 0.8 mt of coke per mt of Zn while emitting vast amounts of contaminated nitrogen derived from the combustion of coke in air. These emissions could be substantially reduced if carbon (or other fossil fuels) were used exclusively as reducing agents and process heat were supplied by an alternative *clean* energy source, e.g., solar energy. Concentrated solar radiation can provide the process heat required to drive this kind of high-temperature endothermic processes [4,5].

Using natural gas (NG) as reducing agent combines in a single process the reforming of methane to produce synthesis gas (syngas) and the reduction of ZnO to produce Zn (Ref. [4] and literature cited therein). The overall reaction is

$$ZnO + CH_4 \rightarrow Zn + 2H_2 + CO. \quad (1)$$

This combined process has three positive features: (i) methane is reformed in the absence of catalysts and, with proper optimization, may be made to produce high-quality syngas with an H_2 to CO molar ratio of 2, which is especially suitable for methanol synthesis; (ii) the evolved gases are sufficiently valuable commodities to justify their collection, eliminating inherent gas emissions to the environment; (iii) performing of ZnO reduction and NG reforming in a single reactor improves energy efficiencies through concurrent high-temperature reactions. The co-production of Zn and syngas, as represented by reaction (1), avoids the chemically derived CO_2 emissions in the traditional carbothermic reduction of ZnO [4]. Furthermore, the use of solar energy upgrades the heating value of the initial reactants by

†Author for correspondence. Fax: + 41-56-3103160; e-mail: aldo.steinfeld@psi.ch

‡Assumptions: zinc production is 85% by electrolysis and 15% in the Imperial Smelting Furnace (ISF) [1]; total CO_2 emissions from electrolysis are estimated assuming 0.87 kg CO_2/kWh$_e$ for coal-fired electricity and energy consumption of 50 GJ/mt Zn produced [2]; total CO_2 emissions from ISF assuming carbon consumption of 0.78 mt C/mt Zn produced [3].

39%. Thus, using this process, solar radiation falling intermittently in the deserts of the earth's sunbelt can be stored as solar chemical fuels for transportation to the world's industrialised and populated centers.

The chemical thermodynamics and kinetics of reaction (1) have been reported in previous studies [6,7]. The chemical equilibrium composition of the system $ZnO + CH_4$ at 1250 K and 1 atm consists of a single gas phase containing Zn (vapor) and a 2:1 molar mixture of H_2 and CO. By applying a shrinking-particle model, the reaction rate in a thermogravimeter reactor (flow of CH_4 over a packed bed of ZnO powder with mean particle size of 1.2 μm) was found to be controlled by gas film diffusion in the Stokes regime with an apparent activation energy of 146 kJ/mol [6]. The theoretical maximum overall efficiency for the conversion of solar energy into the Gibbs free energy of the products via reaction (1) has been assessed for an ideal, closed cyclic system that recycles all materials. Assuming a blackbody solar reactor operated at 1250 K, 1 atm, and with a solar power flux concentration of 2000 suns (1 sun = 1 kW/m^2), maximum efficiencies vary between 40 and 65%, depending on the recovery of the sensible heat from the hot products [7]. These previous studies on the thermodynamics and kinetics of the reaction define the constraints that the chemistry places on the engineering design of a solar chemical reactor.

A novel solar reactor has been designed for conducting reaction (1). A small scale reactor prototype (for 5 kW solar input) has been fabricated and tested in a high-flux solar furnace. The present paper describes the reactor design methodology and presents the engineering aspects of its fabrication. Test results of the first solar measurement campaign are also presented and practical problems encountered during experimentation are discussed.

2. REACTOR ENGINEERING DESIGN OF *SYNMET*

SynMet is a solar chemical reactor designed specifically for the co-production of metallic Zn and syngas starting from ZnO and NG. It is shown schematically in Fig. 1. It consists of an insulated cylindrical cavity (#1), that contains a circular, windowed, aperture (#2) to let in concentrated solar

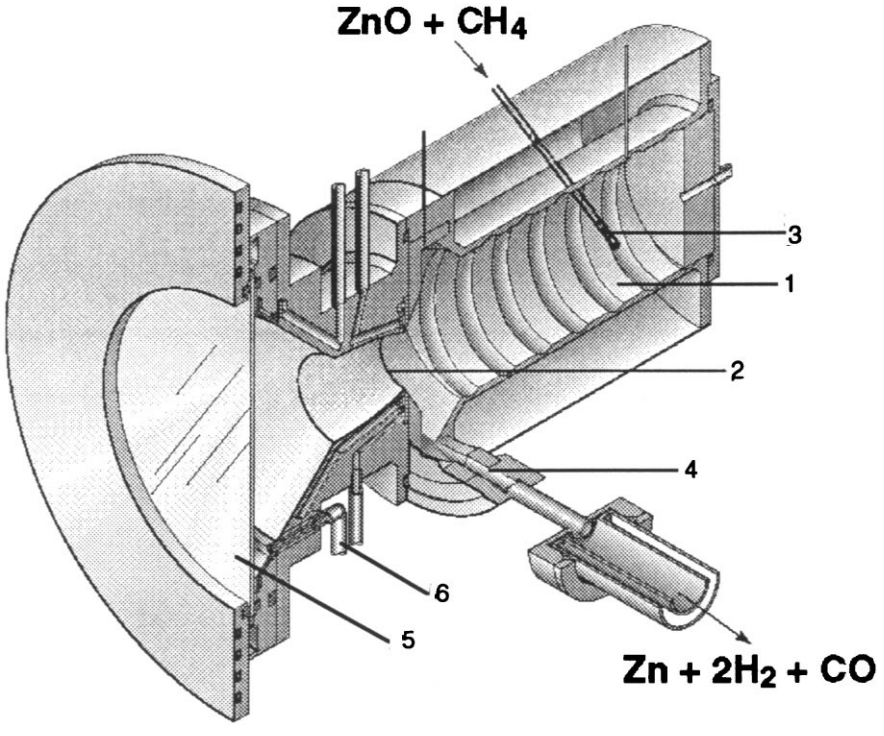

Fig. 1. Schematic configuration of the *SynMet* solar chemical reactor for the coproduction of Zn and syngas. 1, cavity; 2, aperture; 3, inlet port for reactants; 4, outlet port for products; 5, window; 6, auxiliary gas flow. The particles of ZnO are directly exposed to high-flux irradiation, providing efficient heat transfer directly to the reaction site. Energy absorbed by the reactants is used to raise their temperatures to the range 1200-1600 K and to drive the simultaneous reduction of ZnO and reforming of NG. The chemical products exiting the reactor are Zn vapor and syngas.

energy. Particles of ZnO, conveyed in a flow of NG, are continuously injected into the reactor's cavity via a tangential inlet port (#3) located at the back of the cavity. Inside the reactor's cavity, the gas-particle stream forms a vortex flow that progresses towards the front following a helical path. The chemical products, Zn vapor and syngas, continuously exit the cavity via a tangential outlet port (#4) located at the front of the cavity, behind the aperture. The window (#5) is actively cooled and kept clear of particles by means of an auxiliary flow of gas (#6) that is injected tangentially and radially at the window and aperture planes, respectively.

2.1. *Heat transfer*

With this arrangement, the ZnO particles are directly exposed to the high-flux irradiation. Such concept provides efficient radiation heat transfer to the reaction site where the energy is needed, by-passing the limitations imposed by indirect heat transport via heat exchangers. Some of the incoming irradiation undergoes multiple scattering among the particles and multiple reflections within the cavity walls, until it is absorbed by the particles and cavity walls. Other mechanisms of heat transfer to the reactants include infrared radiation by the hot particles and cavity walls, forced convection between the cavity walls and the gas stream, and conduction to ZnO particles that are swept across the hot reactor walls. Vortex (and cyclone) reactors have proven to be efficient devices for the transfer of heat to flows laden with particles [8]. Energy absorbed by the reactants is used to raise their temperature to above about 1200 K and to drive reaction (1).

2.2. *Reactor geometry*

The reactor features a cavity-type receiver geometry. It is basically an insulated enclosure designed to effectively capture incident solar radiation entering through a small opening (the *aperture*). Because of multiple internal reflections, the fraction of the incoming energy absorbed by the cavity exceeds the surface absorptance of the inner walls. Such an effect, called the cavity effect, can be expressed by the apparent absorptance, defined as the fraction of energy flux emitted by a blackbody surface stretched across the cavity opening that is absorbed by the cavity walls. The apparent absorptance has been calculated for cylindrical, conical and spherical geometries having diffuse and specularly reflecting inner walls [9–11]. The larger the ratio of cavity diameter or depth to aperture diameter, the closer the cavity-receiver approaches a blackbody absorber. For example, for a cylindrical cavity having the same relative dimensions as the *SynMet* (ratio of cavity diameter to aperture diameter = 1.7, ratio of cavity depth to aperture diameter = 2), the apparent absorptance is greater than 0.979 for surface absorptance greater than 0.5.

It is important to note that the apparent absorptance is calculated assuming a lambertian directional distribution of the incident radiation. In reality, the power flux distribution will depend on the optics of the concentrator. It is also assumed that the medium inside the cavity does not participate in the radiation exchange, but, in reality, the reactants (especially the particles), absorb, emit and scatter radiation. Nevertheless, Monte-Carlo ray tracing simulations have shown that the apparent absorptance of a cavity-receiver is only weakly affected by the directional distribution of the incident power [11,12]. As the incoming rays undergo multiple isotropic scattering among particles and multiple diffuse reflections within the inner walls, the apparent absorptance becomes less and less dependent on the direction of the incident rays.

2.3. *Reactor sizing*

At temperatures above about 1000 K, the net power absorbed by the cavity-receiver is diminished mostly by radiative losses through the aperture. Thus, the aperture size is the most important dimension for determining the amount of power in and out. The solar energy absorption efficiency of a cavity-receiver $\eta_{\text{absorption}}$ accounts for this phenomenon. It is defined as the net rate at which energy is being absorbed divided by the solar power coming from the concentrator. For a perfectly insulated cavity receiver (no convection or conduction heat losses), it is given by [13]

$$\eta_{\text{absorption}} = (\alpha Q_{\text{aperture}} - \epsilon A_{\text{aperture}} \sigma T^4)/Q_{\text{solar}} \tag{2}$$

The first term in the numerator denotes the total power absorbed and the second term denotes the re-radiation losses; their difference yields the net power absorbed by the reactor. The incoming solar

power is determined by the normal beam insolation, by the collector area, and by taking into account for the optical imperfections of the collection system (e.g., reflectivity, specularity, tracking errors). The capability of the collection system to concentrate solar energy is often expressed in terms of its mean flux concentration ratio over an aperture, normalized with respect to the incident normal beam insolation as follows:

$$\tilde{C} = Q_{\text{aperture}}/IA_{\text{aperture}}. \tag{3}$$

Solar concentration ratios of 1000 are technically feasible in large scale solar collection facilities using present central-receiver and heliostat technology [15]. They can be further increased by improving the optical precision of the heliostat field or by using non-imaging secondary reflectors (e.g. compound parabolic concentrators, often referred to as CPC [16]). Higher $\tilde{C}$ would allow for smaller apertures to intercept the same amount of energy, thus reducing re-radiation losses. Although larger apertures intercept more sunlight reflected from imperfect and imperfectly matched heliostats and concentrators, they also re-radiate more energy. Therefore, the optimum aperture size for maximum $\eta_{\text{absorption}}$ results from a compromise between maximizing radiation capture and minimizing re-radiation losses. It is determined by solving [14]

$$\partial\eta_{\text{absorption}}/\partial r_{\text{aperture}} = 0. \tag{4}$$

For imaging solar concentrators, for which the incident flux-density distribution at the focal plane is close to Gaussian (with maximum flux density F_{peak} and radial standard deviation μ), and further assuming a blackbody cavity-receiver ($\alpha = \epsilon = 1$), Eq. (4) yields the optimum aperture radius

$$r_{\text{opt}} = [-2\mu^2 \ln(\sigma T^4/F_{\text{peak}})]^{0.5}. \tag{5}$$

Eq. (5) serves to guide the determination of the aperture size for maximum efficiency. For example, for a reactor operating at 1400 K and for a solar flux input having the optical characteristics of PSI's solar furnace ($F_{\text{peak}} \approx 2500\ \text{kW/m}^2$ and $\mu \approx 2.5$ cm, which are representative for 75% of full power load), the optimum aperture radius is 5.5 cm. An alternative approach is to determine the size of the aperture so that it intercepts a given incident solar power. Assuming again a Gaussian power flux distribution, the radius of the aperture becomes

$$r_{\text{aperture}} = [-2\mu^2 \ln(1 - Q_{\text{aperture}}/2\pi\mu^2 F_{\text{peak}})]^{0.5}. \tag{6}$$

For example, for a desired input power of 5 kW using PSI's solar furnace, the aperture diameter should be about 6 cm.

Given the total power input, the aperture size, and the operating temperature, one can estimate the power lost by re-radiation and the net power absorbed by the reactants. The mass flow rates of the reactants result from matching the net power absorbed with the enthalpy of the reaction,

$$Q_{\text{reactor,net}} = \dot{m}\Delta H|_{\text{reactants@}T_1,p \rightarrow \text{products@}T_2,p}. \tag{7}$$

Table 1 shows the enthalpy change of the reaction as a function of the total pressure p; the reactants are 1 mol ZnO and 1 mol CH_4, fed at 298 K, and the products are in thermodynamic equilibrium at 1250 K and at 1350 K [17].

Once the mass flow rates are determined, the dimensions of the cavity-receiver are estimated so that the residence time of the reactants inside the reactor chamber is sufficient for the complete reaction (or for a desired reaction extent), as imposed by the kinetics of the reaction. If the reactants are only partially reacted after one pass, they can eventually be recirculated back to the reactor until they are fully reacted.

Table 1. Enthalpy change for $ZnO + CH_4$ @298 $K \rightarrow$ *products* @ 1250 *K*, 1350 *K*.

	T = 1250 K				T = 1350 K
	p = 1 atm	p = 3 atm	p = 5 atm	p = 10 atm	p = 10 atm
ΔH [kJ]	549	545	541	449	554

2.4. *Flow visualization and computational fluid dynamics* (*CFD*)

The reactor design evolved from an initial proposal as a result of flow-visualization experiments and CFD simulations carried out in various geometries and flow configurations. Clear Plexiglas models were built for the purpose of visualising the flow patterns in cold conditions. The initial design had an axial outlet flow and did not perform satisfactorily because of particle sedimentation inside the cavity chamber as well as deposit of dust at the window and CPC. The sedimentation could be minimized to some acceptable levels by having instead tangential inlet and outlet ports at the cavity's back and front respectively, thus creating a stable vortex flow that is able to carry particles along a helical path, regardless of the orientation relative to gravity. In order to increase the residence time of particles inside the reactor chamber and to augment heat transfer between reactants and reactor walls, a spiral groove was machined to guide the particles into a tight helical path rather than the natural coarse helical path. Such a feature

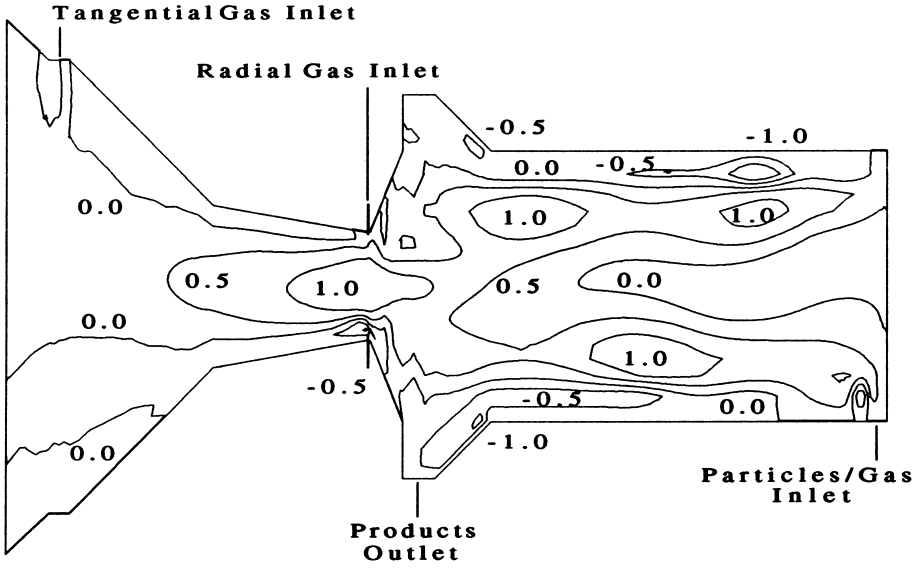

Fig. 2. Wall boundaries and contour lines are shown for constant velocity (interval size 0.5 m/s) for the axial velocity component. Parameters: the main flow at the back inlet port = 27.8 l_n/min; the radial jet flow at the aperture = 13.9 l_n/min; the tangential flow at the window = 9.3 l_n/min; particle mass flow rate = 8.4 g/min. Positive values are for the direction from left to right.

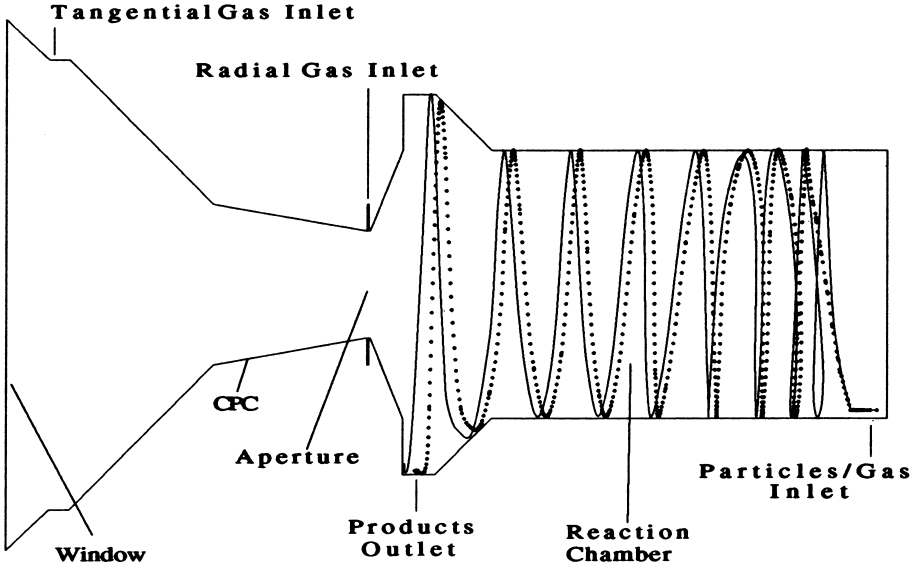

Fig. 3. Boundaries and particle trajectories projected on the vertical plane that contains the reactor axis. Parameters are the same as in Fig. 2. The full line refers to a particle diameter of 10.5 μm and the dotted line to 14.3 μm.

was applied with success in a vortex reactor for the ablative pyrolysis of biomass [18]. A pitch of 3 cm for a reactor tube diameter of 10 cm was found to function properly for fine ZnO powder (0.5–2 μm particles) within a wide range of inlet velocities. The window and CPC were kept clear of particles with the help of auxiliary gas flows (not laden with particles) injected through tangential and radial ports located strategically at the window and aperture planes, respectively (see Fig. 1).

CFD simulations were employed to calculate the velocity field and particle trajectories for different geometries and flow boundary conditions. The Navier-Stokes equations were solved by applying the hybrid differencing schemes and the k-ϵ turbulence model [19]. The motion of the particles in the gas flow was modelled using a discrete trajectory (Langrangian) approach. Optimization was accomplished for minimizing the auxiliary flow while keeping the window and CPC clear of particles. Fig. 2 shows the results of a 3-dimensional calculation of the isothermal gas flow. It is observed that, near the axis, the vortex flow moves in the positive direction (from left to right), primarily as a result of the auxiliary window flow, while close to the walls the vortex flow moves in the opposite direction (from right to left) as a result of the main gas/particle stream that progresses towards the front following a helical path. This helical path is illustrated by the particle trajectories in Fig. 3. Larger (and heavier) particles follow a tighter spiral path, while the smaller (and lighter) particles follow the gas flow streamlines more closely. For the given gas and particles mass flow rates, no particles escape through the aperture.

2.5. *Fabrication of reactor prototype*

A 5-kW prototype was fabricated and is shown in Fig. 4. The cavity body is a 10 cm diameter, 20 cm length cylinder made of heat-resistant steel alloy (m.p. = 1670 K). In front of the 6 cm aperture, the cavity-receiver was equipped with a diverging conical aluminum funnel so that the window could

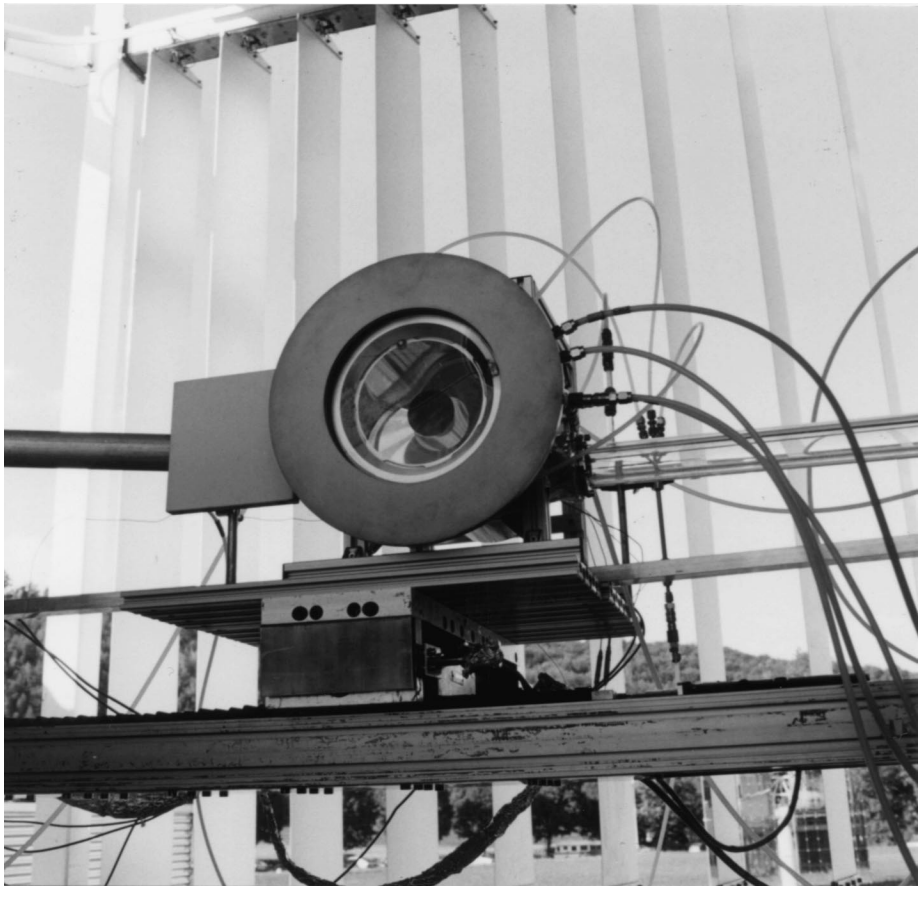

Fig. 4. Photograph of the 5-kW solar reactor tested at the PSI solar furnace. The front face contains a 6-cm diameter aperture and a 24-cm diameter quartz window. The water-cooled target seen on the left is the Lambertian target used for measuring the solar power flux intensity optically. The water-cooled Pyrex condenser seen on the right is used for distillation of Zn vapor from the exiting gaseous products.

be mounted 7 cm in front of the focal plane where the radiation intensity is about 10 times smaller and dust deposition is unlikely to occur. The window is a 24 cm diameter, 0.3 cm thick clear fused quartz disc. It has a nominal transmissivity of 0.94 in the 0.26–3.6 μm wavelength range, but its transmissivity drops to 0.20 in the 2.5–3.6 μm range. Thus, the quartz may absorb a substantial fraction of the infrared radiation emitted by the reactor in that range. Nevertheless, the physical and thermal properties of quartz should permit its continuous use up to 1300 K. The window is suspended in 3 o-rings that permit thermal expansion in any direction, and is mounted in a water-cooled copper ring that also serves as a shield for spilled radiation. In some of the experiments, we incorporated a water-cooled, diamond-machined aluminum CPC, which augmented the flux concentration by a factor of 2. Thus, for a given input power, the aperture size was reduced by half, and consequently, the re-radiation losses were reduced by half.

3. SOLAR EXPERIMENTAL PROGRAM

Experimentation was conducted at the PSI solar furnace.[†] The optical set-up is shown schematically in Fig. 5. The solar furnace is a two-stage concentrating system consisting of a sun-tracking heliostat of 51.8 m^2 area, 100 m focal length, and a stationary parabolic dish of 5.7 m^2, 1.9 m focal length, delivering up to 15 kW with a peak concentration ratio of 3500 suns (1 sun = 1 kW/m^2). The power delivered to the reactor is controlled by a venetian blind-type shutter, located between the heliostat and the concentrator. Power flux intensities are measured optically by recording the image of the sun on an Al_2O_3-coated Lambertian target with a calibrated charge-coupled device (CCD) camera. The CCD camera is also used to monitor continuously the position of the reactor relative to the flux map, so that the regions of maximum flux intensity are intercepted.

The complete experimental reactor system, including the peripheral components and the measuring

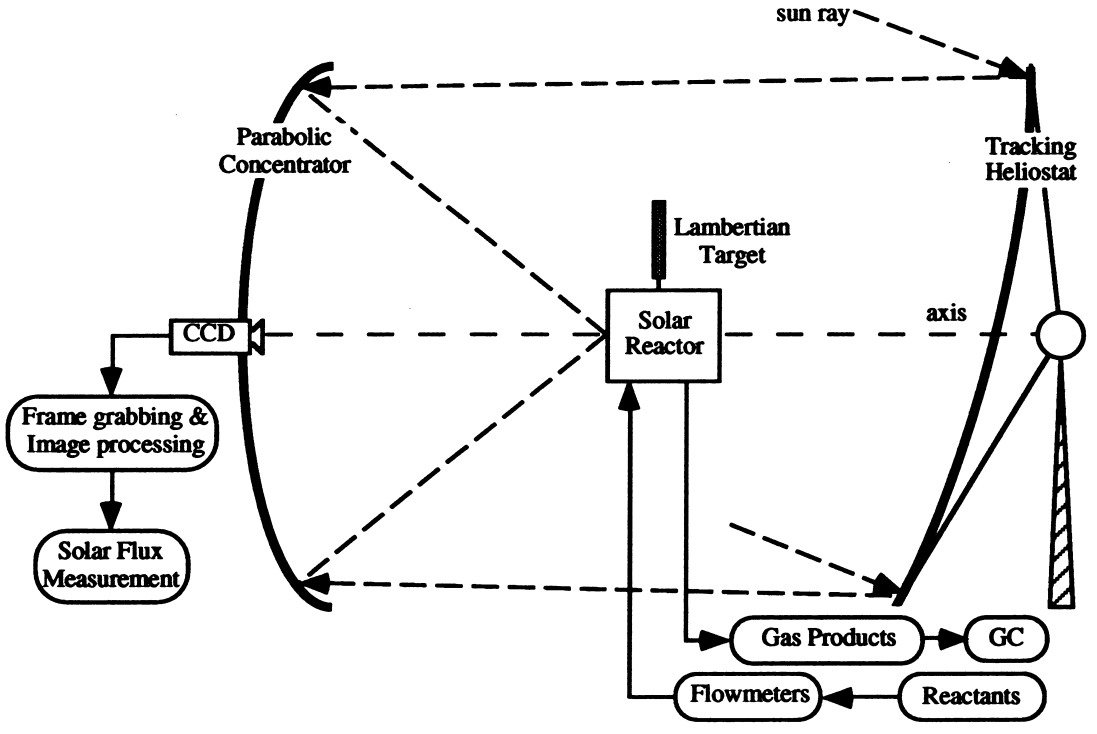

Fig. 5. Schematic of the PSI solar furnace (the dimensions are not to scale). It is a two-stage concentrating system consisting of a sun-tracking heliostat and a stationary parabolic dish delivering up to 15 kW with a peak concentration ratio of 3,500 suns.

[†]Technical information on the PSI solar furnace may be obtained at www1.psi.ch/www__f5__hn/Solar/solar__home.html

and control instrumentation, is shown schematically in Fig. 6. ZnO particles are fed mechanically into the main gas stream by means of a spiral-type feeder, just before injection into the reactor. Gas mass flow rates and concentration of CH_4 in Ar are electronically controlled. Both gas and particles are injected at ambient temperature and at slightly above atmospheric pressure. If preferred, the main gas stream can be pre-heated electrically to simulate heat exchange with the exiting hot products. Reactor wall temperatures are measured with thermocouples type-K inserted in the wall and not exposed to the direct irradiation. Pressure inside the reactor is also electronically monitored and its value is limited by a pressure release safety valve. Reaction products exiting the reactor flow through a 1 m long water-cooled Pyrex condenser, where some portion of the Zn condenses. Downstream, a battery of filters collects the remaining particles, derived either from Zn condensation, Zn re-oxidation, or unreacted ZnO. The composition of the product gases is quantitatively analyzed by gas chromatography. The nature of the solid products collected at the condenser and at the filters is analyzed by X-ray powder diffraction. The amount of Zn produced is determined by reacting the solid products with HCl and measuring the volume of hydrogen evolved. The accuracy of such technique is ± 6%.

3.1. *Preliminary solar experimental results*

ZnO powder (Alfa Nr. 85113) with a mean particle size of 0.4 μm was fed at a rate of about 5 g/min. Inlet gas flow rate, for various concentrations of CH_4 in Ar, was in the 15–20 l_n/min[†] range; the auxiliary flow without particles was in the range of 20–30 l_n/min. The loading ratio of particles to gas was kept below the stoichiometric ratio [as given by Eq. (1)] to avoid plugging or sedimentation, and to protect the window from particle deposition. Excess methane was between 5 and 25 times more than the stoichiometric amount. During a typical experiment, the reactor was solar-heated to the desired temperature under a flow of Ar or N_2 and then isothermally subjected to the reacting flow. The reactor was exposed to peak solar fluxes of about 2000 suns; higher flux intensities were possible but were avoided to prevent overheating. Maximum reactor wall temperatures, under approximate steady-state conditions, ranged between 1000–1600 K and were measured typically at the center top. As soon as particles were

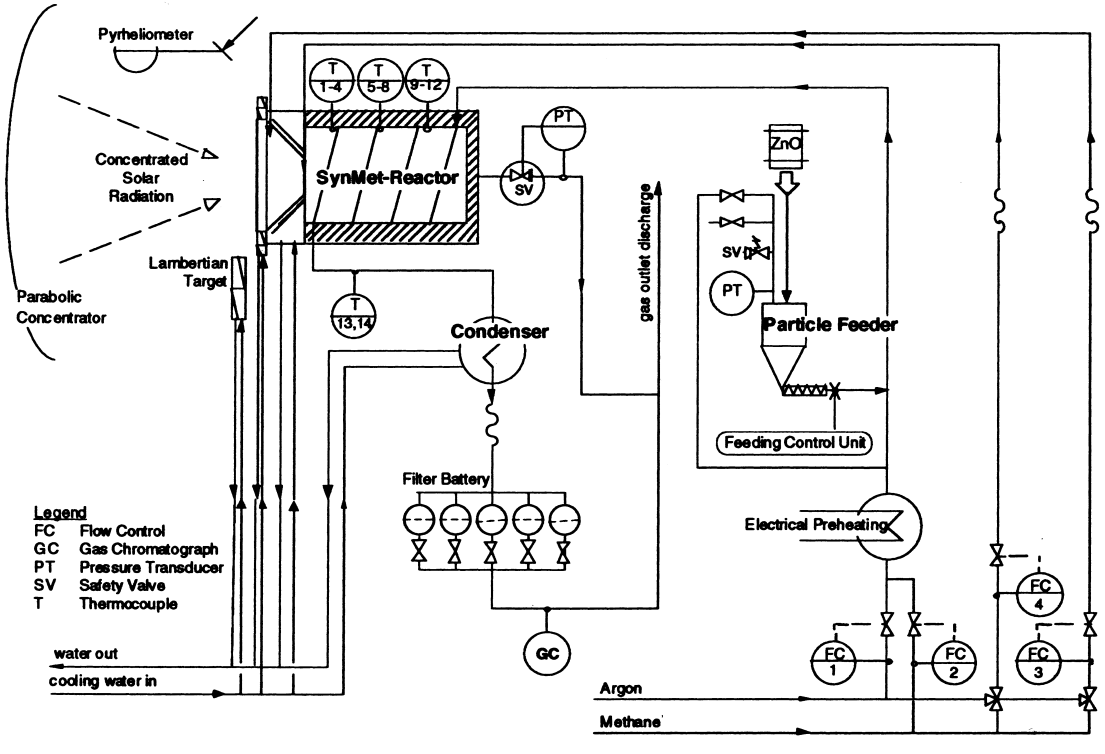

Fig. 6. Flow sheet diagram of the complete experimental set-up. The reactor operates in a continuous mode; the reactant mass flow rates and inlet solar power are controlled.

[†]l_n means liters at normal conditions; mass flow rates are calculated at 273 K and 1 atm.

injected into the hot reactor, wall temperatures dropped by about 100–150 degrees, as a result of the endothermic reaction and of the shielding effect of the particles. The particles of ZnO were forced to the walls by the centrifugal force and were efficiently heated by contact with the hot walls (besides being heated by direct absorption, as described in the *Heat Transfer* section). Wall temperatures were not uniform; close to the aperture, where the main and cold auxiliary flows are mixed, temperatures were typically 100–250 degrees lower than those at the center top. A more uniform temperature distribution may be obtained by preheating both flows. Temperatures were controlled indirectly by controlling the amount of incoming power flux with the furnace's shutter. Zn vapor exiting the reactor was distilled in the water-cooled condenser.

The chemical conversion[†] of ZnO to Zn obtained after a single pass of about 3 seconds is shown in Table 2; the maximum reactor wall temperature and the CH_4 concentration of the inlet gas are also indicated. As expected, best results were obtained at higher temperatures, higher CH_4 concentrations, and when the reactants were pre-heated. Conversions of over 50% were obtained when the maximum wall temperature exceeded 1300 K. Up to 90% Zn yield was obtained when the maximum wall temperature was 1600 K, however such high temperature approaches the maximum operating temperature of the materials of construction. Mean particle size of the Zn collected in the condenser was typically 2 μm; all particles were smaller than 10 μm. No carbon deposition was detected among the products. The conversion of methane to syngas was incomplete because the reaction was effected with considerably excess methane. Complete conversion of ZnO and CH_4 may be achieved by increasing the operating temperature and the residence time, or by recirculating the unreacted effluents through the reactor. The use of methane-reforming catalysts, such as Ni, Rh, and others, will most probably result in higher rates of reaction, but their use would be subjected to the feasibility of recovering them from the products.

Scanning electron micrographs (S.E.M.) were obtained from the reactants and the products for the solar run using 10% CH_4-Ar and at a maximum wall temperature of 1280 K. Figure 7 shows ZnO powder used as reactant; particles underwent partial sintering while being dried for 2 hours at 873 K. Fig. 8 shows the products collected at the water-cooled condenser where the average Zn yield obtained was 26.1%. It is observed that Zn grew in plane layers, resulting from the condensation of Zn vapor when coming in contact with the cold surface. Figure 9 shows the products collected in the form of aerosol at the filter downstream from the condenser, where the average Zn yield was 30%. The spherical particles of 1–4 μm resulted from the condensation of Zn vapor and contain more than 70% Zn (as determined by Energy Dispersive X-ray spectroscopy, EDX). The remaining particles are mostly unreacted ZnO that were carried away by the gas flow.

Table 2. Maximum wall temperature, CH_4 concentration in the inlet gas, and Zn yield obtained in solar runs.

T_{max} [K]	% CH_4-Ar	Zn yield [%]
1000	100%	0.9
1050	10%	7.5
1150	4%	17.3
1175	22%	32.2
1200	10%	9.9
1200	10%	10.0
1200	24%	36.1
1230	100%	40.3
1250	10%	15.3
1250	100%	43.4
1260	10%	15.6
1280	10%	26.1
1350	10%	54.6
1410	100%	78.0
1550	10%	85.0[†]
1600	10%	90.0[†]

[†]The reactants were electrically preheated to 800 K.

[†]Chemical conversion (or zinc percentage yield) is defined as the amount of zinc produced in the solar furnace divided by the maximum amount of zinc that would have been recovered if the reaction had gone to completion.

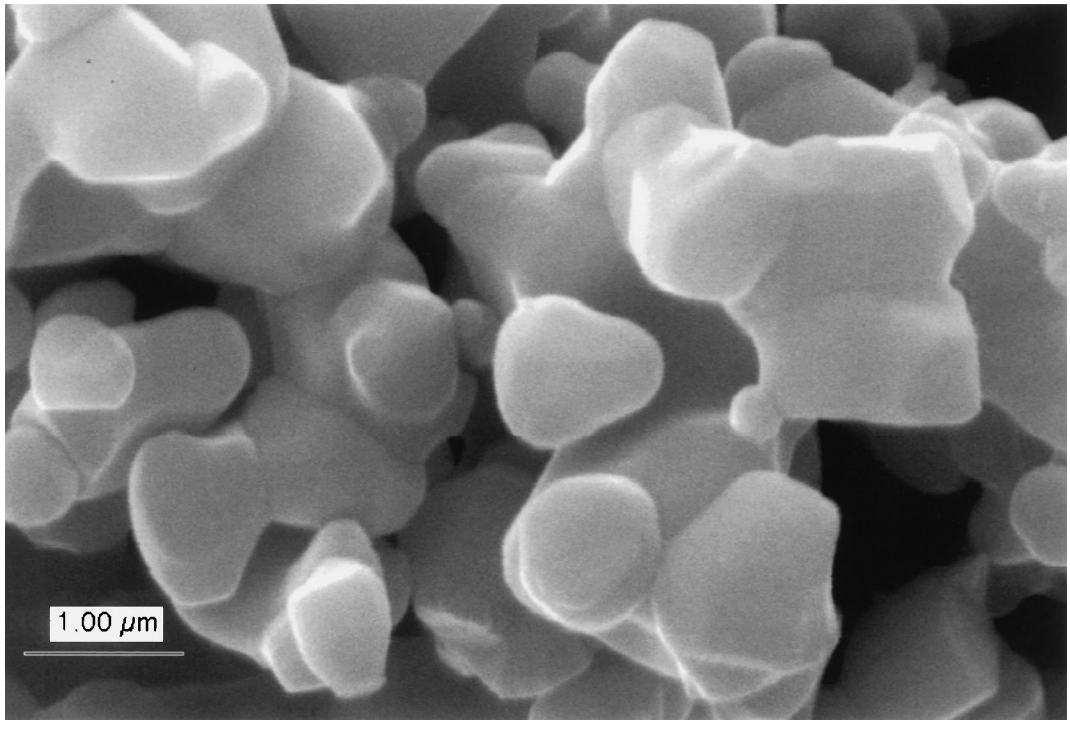

Fig. 7. S.E.M. of the reactant ZnO powder (Alfa Nr. 85113) after drying for 2 hours at 873 K.

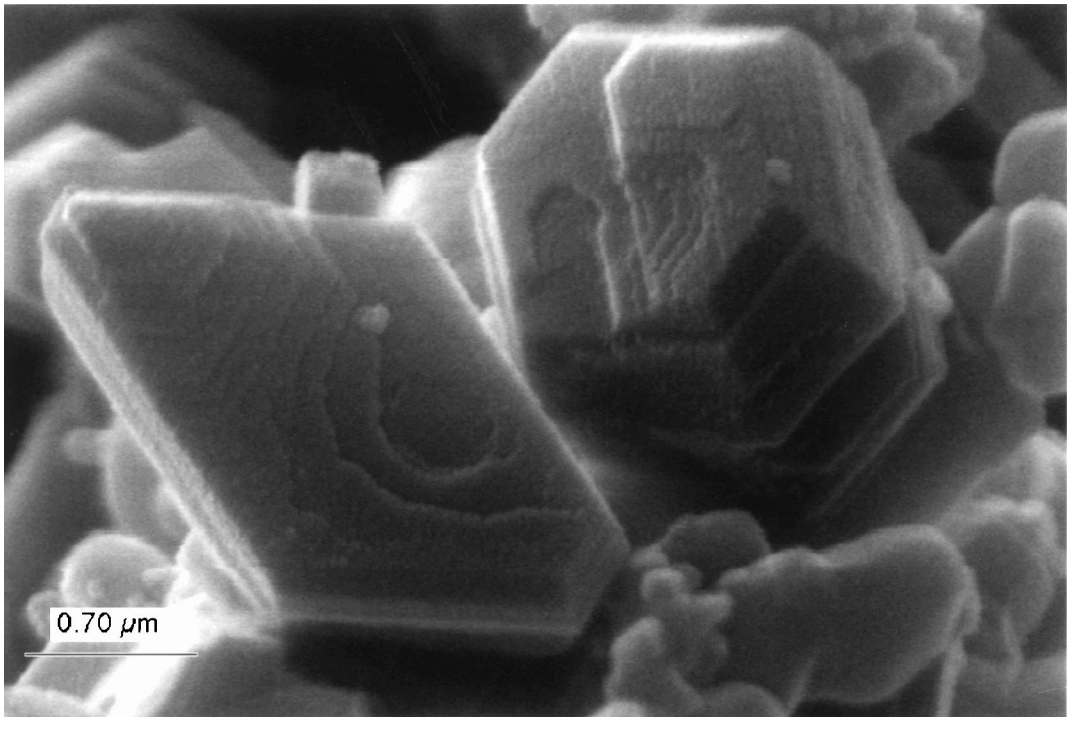

Fig. 8. S.E.M. of products collected at the water-cooled condenser. Zn grew in plane layers as a result of the condensation of Zn vapor.

3.2. *Some observations about windows and CPCS*

The window worked well during the course of the experiment. But, while trying to minimize the auxiliary flows, some Zn vapor would diffuse to the front, condense at the window, and decrease its transmissivity. Windowed reactors offer the advantage of direct irradiation of the reactants. However,

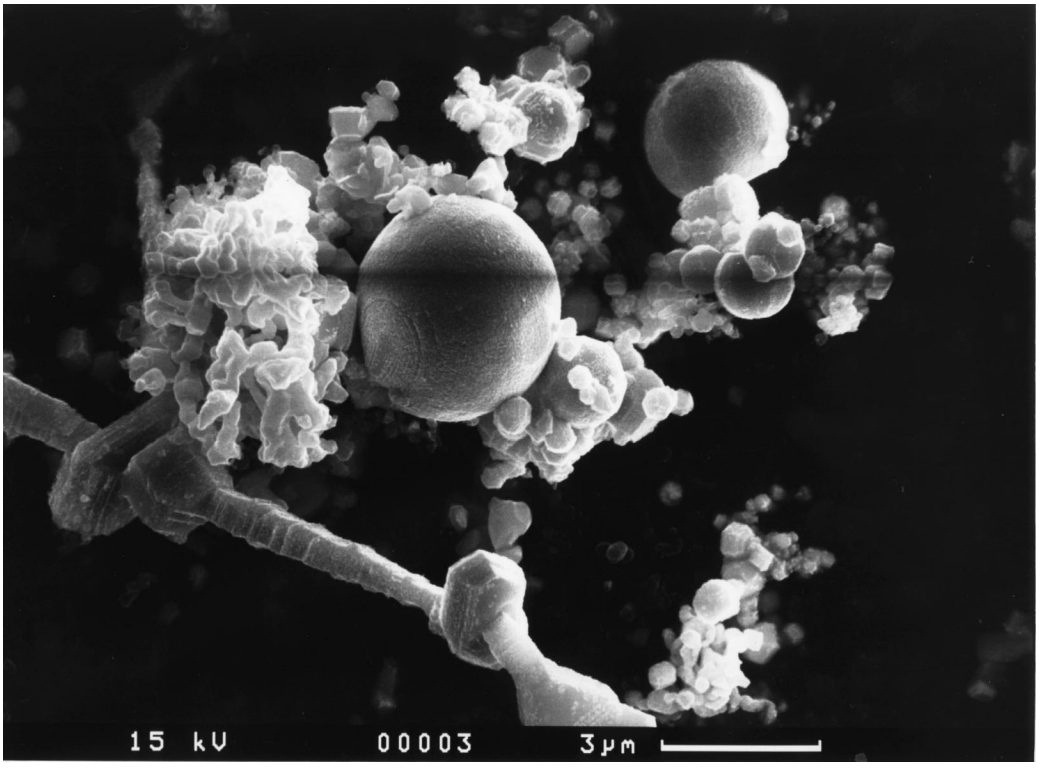

Fig. 9. S.E.M. of products collected at the filter downstream from the condenser. The large spherical particles (of 1–4 μm) resulted from condensation and solidification of Zn vapor. The remaining particles are mostly unreacted ZnO.

windows that operate in the presence of severe atmospheres such as particles and condensing vapors require aerodynamic protecting flows. Unless such auxiliary flows serve also the function of reactants in gas-solid reactions, the energy conversion efficiency will be significantly decreased due to the energy requirement for separation and re-circulation processes. For example, for the ZnO + CH_4 reaction, methane should be used to protect the window. Another gas-solid reaction for which *SynMet* may find application is the solar gasification of carbonaceous materials (e.g., coal and biomass). For gasification processes using steam as the gasifying agent, it would be preferable to use steam for protecting the window. The same problem affects the implementation of CPCs in severe gas-solid reacting environments. Since the concentrated light exits the CPC with a view angle of 180°, the CPC exit should be positioned exactly at the aperture plane. In this critical zone, ZnO particles or Zn vapor may be deposited and cause deterioration of the CPC reflectivity. Similar to the window protection, the CPC can also be protected by having an auxiliary flow that prevents dust deposition but, unless such a flow acts as a reactant, it will affect the reactor efficiency significantly. The use of CPCs and windows in gas-particle environments should be further investigated.

4. CONCLUDING REMARKS

We have presented the engineering design of a solar chemical reactor for conducting the simultaneous ZnO-reduction and CH_4-reforming. The vortex flow configuration was proven to be an efficient reactor concept for the transfer of heat to gas flows laden with particles and for conducting fast gas-solid thermochemical processes. First tests conducted in a solar furnace using a small scale reactor prototype yielded up to 90% chemical conversion to Zn in a single pass. Technical feasibility for the proposed solar process has been demonstrated. There is still room for improvement and optimization.

The use of high-temperature solar process heat for the co-production of zinc and synthesis gas offers the possibility of reducing greenhouse-gas and other pollutant emissions produced in conventional fossil-fuel-based processes. Furthermore, it provides an efficient conversion path of solar energy into storable and transportable chemical fuels.

Present market prices for Zn are about 1000 US$/mt. The cost of this valuable metal is directly tied to the cost of the energy required to produce it: assuming an energy consumption of 35–50 GJ/mt when produced electrolytically [1] and a power cost of 0.05 US$/kWh, the cost of the energy represents between 40–70% of the value of Zn. The cost of solar producing Zn from ZnO would have to be compared with the economics of conventional fossil-fuel-based processes. Once the cost of energy will account for the environmental externalities from burning fossil fuels (e.g. depletion, CO_2 mitigation, and pollution abatement), solar energy will become a favorable competitive long term prospect.

Acknowledgements—We gratefully acknowledge financial support from the BEW-Swiss Federal Office of Energy. We thank P. Haueter and T. Seitz for technical support at the solar furnace, and A. Frei, A. Estermann, and P. Widmer for the chemical analyses. We also thank R. Palumbo for a critical review of the paper.

REFERENCES

1. *Encyclopedia of Chemical Technology*, 3rd ed., John Wiley and Sons, NY, 1985.
2. Hassmann, K. and Kühne, H. M., *Int. J. Hydrogen Energy*, 1993, **18**, 635.
3. Kola, R., in *Proceedings of the International Symposium on Extractive Metallurgy of Zinc*, Tokyo, 14-16 October, 1985, pp. 573–596.
4. Steinfeld, A., *Energy-The International Journal*, 1977, **22**, 311.
5. Steinfeld, A., Kuhn, P., Reller, A., Palumbo, R., Murray, J. and Tamaura, Y., *Int. J. Hydrogen Energy*, 1998, **23**, 767.
6. Steinfeld, A., Frei, A., Kuhn, P. and Wuillemin, D., *Int. J. Hydrogen Energy*, 1995, **20**, 793.
7. Steinfeld, A., Larson, C., Palumbo, R. and Foley, M., *Energy-The International Journal*, 1996, **21**, 205.
8. Szekely, J. and Carr, R., *Chemical Engineering Science*, 1966, **21**, 1119.
9. Lin, S. and Sparrow, E., *J. Heat Transfer*, 1965, 299.
10. Siegel, R. and Howell, J. R., *Thermal Radiation Heat Transfer*, 3rd ed., Hemisphere Publishing Corporation, Washington, DC, 1992.
11. Steinfeld, A., *Int. J. Heat Mass Transfer*, 1991, **34**, 1895.
12. Steinfeld, A., *Wärme-und Stoffübertragung*, 1993, **28**, 65.
13. Fletcher, E. A. and Moen, R. L., *Science*, 1977, **197**, 1050.
14. Steinfeld, A. and Schubnell, M., *Solar Energy*, 1993, **50**, 19.
15. Winter, C. J., Sizmann, R. L. and Vant-Hull, L. L., *Solar Power Plants*, Springer-Verlag, Berlin, 1991.
16. Welford, W. T. and Winston, R., *High Collection Nonimaging Optics*, Academic Press, San Diego, 1989.
17. Reynolds, W. C., *The Element Potential Method for Chemical Equilibrium Analysis*, Stanford University, Palo Alto, USA, 1986.
18. Diebold, J. and Scahill, J. W., *Developments in Thermochemical Biomass Conversion*, Banff, Canada, 1997, pp. 242–252.
19. Meier, A., Ganz, J. and Steinfeld, A., *Chemical Engineering Science*, 1996, **51**, 3181.

NOMENCLATURE

$A_{aperture}$ = Area of reactor aperture (m^2)
C = Mean flux solar concentration
ΔH = Enthalpy change (kJ)
F_{peak} = Peak solar flux intensity (kW/m^2)
I = Normal beam insolation (kW/m^2)
p = Pressure (atm)
$Q_{aperture}$ = Incoming solar power intercepted by $A_{aperture}$ (kW)
$Q_{reactor,net}$ = Net power absorbed by the solar reactor (kW)
Q_{solar} = Total solar power coming from the concentrator (kW)
$T_{reactor}$ = Nominal cavity-receiver temperature (K)
$r_{aperture}$ = Radius of reactor aperture (m)
r_{opt} = Optimum radius of reactor aperture for maximum $\eta_{absorption}$ (m)
α, ϵ = Apparent absorptance and emittance of the solar cavity-receiver
$\eta_{absorption}$ = Solar energy absorption efficiency
μ = Radial standard deviation of Gaussian flux distribution (m)
σ = Stefan-Boltzmann constant (5.6705×10^{-8} $Wm^{-2}K^{-4}$)